Instability and transition of a Mach-5.8 flat plate boundary layer over a thermo-mechanically compliant panel

By D. J. Bodony†

High-speed flight vehicles generate thermo-mechanical loads on the supporting structure that may induce static and dynamic deformations which, in turn, change the flow field. We quantitatively explore this scenario in the context of the fluid-thermal-structural coupling experienced by infinitesimally-small disturbances known to exist in otherwise laminar boundary layers grazing nominally flat surfaces. Both convective and global stability analyses are conducted. For panels of thickness h^*, the boundary layer Blasius lengthscale ℓ^*, and local streamwise Reynolds number $\mathrm{R} = \sqrt{U_\infty^* x^*/\nu_\infty^*}$, the non-dimensional parameter $h^*\mathrm{R}/\ell^*$ usefully parameterizes the conditions under which dynamically significant interaction is possible.

1. Introduction

A gap exists in understanding the importance of aerodynamic surface compliance, such as on outer mold line surfaces of flight vehicles, and on the instability, transition, and turbulence found in the grazing flow. Carpenter *et al.* (2001) suggest that there is little possibility for any meaningful interaction between an aerodynamic surface and boundary layer instabilities because of the significant density mismatch between the structure and the fluid. On the other hand, aircraft manufacturers have identified several scenarios in which fluid-thermal-structural interaction (FTSI) creates design-critical uncertainties, including in estimating boundary layer transition (Zuchowski 2012). We seek, therefore, to quantitatively understand how FTSI can impact boundary layer instabilities and, ultimately, vehicle design.

Detailed investigations of FTSI at conditions relevant to high-speed, e.g., hypersonic, flight vehicles are rare. At marine conditions, there exists a substantial literature on boundary layer–structure coupling (Kramer 1957, 1960*a*,*b*; Carpenter & Garrad 1985, 1986; Lucey & Carpenter 1995; Wiplier & Ehrenstein 2001), including the review by Carpenter *et al.* (2001). At hypersonic flight conditions, vehicle-scale analyses using reduced-order models have been conducted (Thuruthiamatta *et al.* 2002; Friedmann *et al.* 2004; Culler & McNamara 2010), with some work recently on one-way-coupled estimates of transition location on the thermal-structural response of a panel (Riley *et al.* 2014; Riley & McNamara 2016) using engineering models. Detailed, systematic studies of FTSI-influenced boundary layer transition do not exist. The direct numerical simulation study of Ostoich *et al.* (2013) studied FTSI modification to turbulence, but, while it remains the only of its kind, it did not address boundary layer stability.

In this report we document the application of convective and global stability analyses applied to compressible boundary layers grazing a nominally flat, compliant, thin panel.

† Department of Aerospace Engineering, University of Illinois at Urbana-Champaign

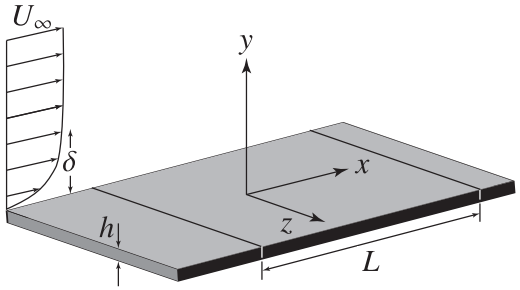

FIGURE 1. Schematic of linear stability problem.

Our goals are (a) to develop the stability analysis tools and (b) to deduce an approximate metric that could be useful in quickly assessing whether surface compliance can meaningfully affect boundary layer instabilities. Following a description of the problem, an order-of-magnitude estimate is provided before convective and global stability analyses are discussed.

2. Base state and perturbation equations

We focus attention on the fundamental FTSI scenario of a compressible, self-similar boundary layer grazing a nominally flat, compliant panel. A typical geometry is shown in Figure 1 where a boundary layer with free-stream velocity U_∞^*† the no-slip and thermal compatibility equations applied at the deformed surface $y = \eta(x, z)$ become, when linearized with respect to the undeformed surface at $y = 0$,

$$u' + \eta \frac{\partial \overline{u}}{\partial y} = 0, \quad v' = \frac{\partial \eta}{\partial t} \tag{2.1}$$

and

$$T_f'(x, 0, z, t) = T_s'(x, 0, z, t), \quad k_f \frac{\partial T_f'}{\partial y} = k_s \frac{\partial T_s'}{\partial y}. \tag{2.2}$$

In addition, the bottom of the panel is assumed to lie within a constant temperature bath so that $T_s'(x, -h, z, t) = 0$. For the global stability problem the compliant panel has a finite length L with clamped boundary conditions that ensure $\eta = 0$ and $\partial\eta/\partial x = 0$ at both ends.

3. Order-of-magnitude analysis

It is instructive to consider the orders of magnitude involved when fluid-borne waves may couple to panel-borne waves. In this way we evaluate the case when boundary layer waves possibly interact with bending waves in the panel. Temporal and streamwise homogeneity requires that both waves have the same temporal frequency and streamwise wavenumber and, therefore, phase velocity c_{ph}. Setting $c_{ph,f}^* = \beta U_\infty^*$, for $\beta \in [0.6, 1.2]$, covers a wide range of fluid waves (e.g., Tollmien-Schlichting, slow and fast Mack modes). In the panel, bending waves have phase speed $c_{ph,s}^* = \sqrt{\omega^* h^* c_L^*/12}$, where $c_L^* = \sqrt{E^*/[\rho_s^*(1-\nu^2)]}$ is the longitudinal wavespeed in an otherwise infinite solid. Equating $c_{ph,f}^* = c_{ph,s}^*$ and introducing the boundary layer-based nondimensional

† Dimensional quantities are denoted with a superscript *

frequency $F = \omega^* \nu_\infty^* / U_\infty^{*2}$ yields the estimate

$$\frac{h^* \mathrm{R}}{\ell^*} = \frac{12\beta^2 \mathrm{M}_\infty^2}{F(c_L^*/c_\infty^*)}, \tag{3.1}$$

where $\mathrm{R} = \sqrt{\mathrm{Re}_x} = \sqrt{U_\infty^* x^* / \nu_\infty^*}$ is the square root of the streamwise distance Reynolds number for a boundary layer that starts at $x^* = 0$ and $\ell^* = x^*/\mathrm{R}$ is the Blasius lengthscale. The right-hand side of Eq. (3.1) is a function of the flow Mach number, the frequency of the disturbance, and the ratio of wavespeeds in the solid and in the fluid. Though only an estimate, Eq. (3.1) incorporates many important physical phenomena excluding, of course, the effect of boundary conditions.

Consider applying Eq. (3.1) to the boundary layer growing on an otherwise flat panel on a vehicle flying at 100,000 ft. altitude. Using material properties from the nickel-based metallic alloy Hastelloy-X (used on the SR-71) shows that fore portions of the vehicle satisfy $h^* < 1$ mm over a range of Mach numbers from 2–12. As aircraft skin panels are typically 0.5–1.0 mm thick, this estimate suggests possible dynamically important interaction.

4. Convective stability analysis

A more quantitative estimate of FTSI-induced boundary-layer stability is obtained by introducing the normal mode assumption that all disturbances in the fluid are described by $q'(x, y, z, t) = \hat{q}(y) \exp\{i(\alpha x + \beta z - \omega t)\}$ for real-valued frequency ω and spanwise wavenumber β. The panel deformation is assumed to similarly satisfy $\eta(x, z, t) = e\hat{t}a \exp\{i(\alpha x + \beta z - \omega t)\}$. After introducing the normal mode assumption into the linearized disturbance equations, the complex eigenvalue α is determined through fixed-point iteration of the boundary conditions in Eq. (2.1).

Applying the convective stability analysis to a Mach 5.8 boundary layer growing on an otherwise flat plate made of Hastelloy-X at a Reynolds number of $\mathrm{R} = 1{,}000$ is shown in Figure 2 as a function of frequency F and panel thickness relative to the local Blasius lengthscale ℓ^*. From the figure it appears that the instability growth rate $-\alpha_i^* \delta_0^*$ becomes sensitive to the panel flexibility when $h^*/\ell^* < 10^{-1}$. Further, the FTSI-induced changes cause higher growth rates over the second Mack mode while reducing the growth rate of the first Mack mode.

A more detailed measure of the change in the instability with increasing panel flexibility is shown in Figure 3 for three values of $h^*\mathrm{R}/\ell^*$ for the same Mach 5.8 boundary layer grazing a Hastelloy-X panel. The growth rate as functions of F and R is given for the case of $\beta = 0$. It is clear that Mack's second mode is amplified as $h^*\mathrm{R}/\ell^*$ decreases. Furthermore, there is some stabilization of low F modes as the panel flexibility promotes instability around the F-R band centered on the rigidly unstable modes.

5. Global stability analysis

Panel boundary conditions dramatically impact their response to external forcing (Dowell 1970). Including their presence in the stability analysis breaks the streamwise homogeneity assumption used in the previous section, so we resort to a global stability analysis where fluid disturbances $q'(x, y, z, t)$ are written as $\hat{q}(x, y) \exp\{i\beta z + \sigma t\}$ for real-valued spanwise wavenumber β and complex-valued temporal growth rate σ. The panel deformation is, likewise, written as $\eta(x, z, t) = \hat{\eta}(x) \exp\{i\beta z + \sigma t\}$.

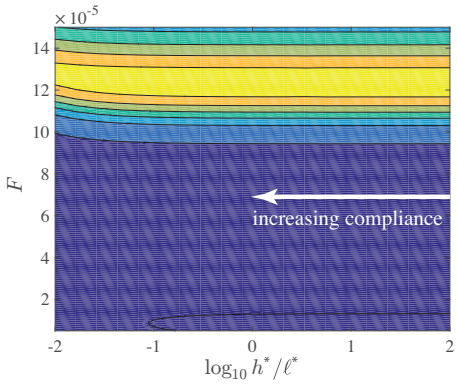

FIGURE 2. Contours of $-\alpha_i^* \delta_0^*$ as a function of panel thickness h^* for a Mach 5.8 boundary layer at R = 1000, $\beta = 0$ for Hastelloy-X. Contour levels are logarithmically spaced between $[10^{-5}, 10^{-1}]$.

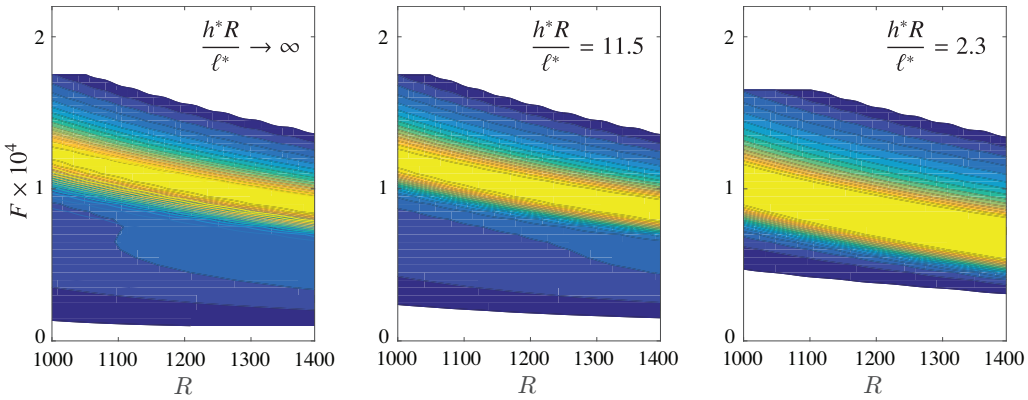

FIGURE 3. Contours of $-\alpha_i^* \delta_0^*$ as functions of F and R for a Mach 5.8 boundary layer with $\beta = 0$ for Hastelloy-X. Contour levels are logarithmically spaced between $[10^{-5}, 10^{-1}]$.

The discrete global stability problem is constructed as follows. The linearized compressible Navier-Stokes equations are discretized using summation-by-parts (SBP) finite difference operators and simultaneous-approximation-term (SAT) boundary conditions as described in Bodony & Natarajan (2012). The panel discretization uses fourth-derivative SBP operators and SAT boundary conditions (Mattsson & Werpers 2016) applied to

$$\sigma^2 \hat{\eta} + \frac{B}{m_s}\left[\frac{\mathrm{d}^4\hat{\eta}}{\mathrm{d}x^4} - 2\beta^2\frac{\mathrm{d}^2\hat{\eta}}{\mathrm{d}x^2} + \beta^4\hat{\eta}\right] + B^{-1}\hat{p}(x,0) = 0, \tag{5.1}$$

and subject to $\hat{\eta} = \mathrm{d}\hat{\eta}/\mathrm{d}x = 0$ at $x = 0, L$ (see Figure 1). Combining Eq. (5.1) with the discretized fluid equations and boundary conditions yields a quadratic eigenvalue problem of the form $(\sigma^2\mathcal{M} + \sigma\mathcal{N})\hat{w} = \mathcal{A}\hat{w}$, where $\hat{w} = [\hat{q}, \hat{\eta}]^T$ is the composite vector of unknowns and $\mathcal{A}$ is the composite discrete operator combining the fluid equations, the panel equation, and their boundary conditions. Though sparse, $\mathcal{A}$ is block full due to FTSI through the boundary conditions and panel equation. After the transformation $\hat{z} = [\hat{w}^T, \sigma\hat{w}^T]^T$, a standard eigenvalue problem $\sigma\hat{z} = \tilde{\mathcal{A}}\hat{z}$ is constructed and solved following the PETSc-SLEPc procedure outlined in Bodony & Natarajan (2012).

A first application of the global stability solver for FTSI used the spatially-developing

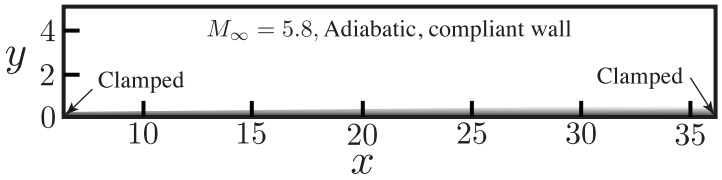

FIGURE 4. Spatial domain used in global stability solution. The inflow and outflow values of R are 1000 and 1700, respectively, and correspond to locations of clamped-clamped boundary conditions.

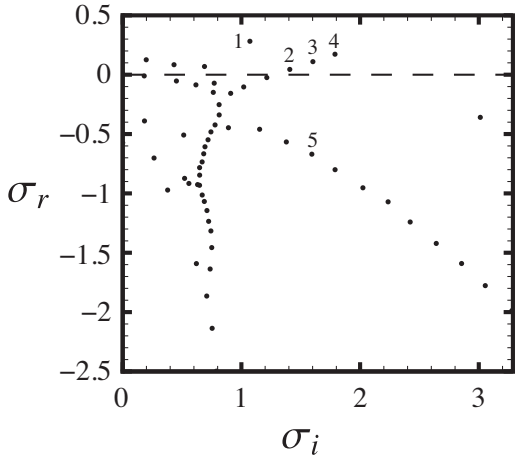

FIGURE 5. Discrete spectrum of the FTSI-coupled global stability solver for the case described in figure 4. Identified modes are shown in figure 6.

Blasius boundary layer at Mach 5.8 in the domain of R $\in [R_{in}, R_{out}] = [1000, 1700]$, as shown in Figure 4. Again, Hastelloy-X is used for the material properties, and the value of $h^* R_{in}/\ell^*_{in} = 10$ is chosen for the panel thickness to ensure measurable effects in the FTSI-influenced results.

Sample results are shown in Figures 5 and 6 for the spectrum and modes, respectively. The five modes identified in Figure 5 are shown individually in Figure 6, with contours of the real part of the vertical velocity shown above the corresponding panel displacement. The presence of several branches in the spectrum can be observed, including seven unstable modes. The most unstable mode, mode 1, is shown in Figure 6(a), and is representative of a fluttering panel as simulated by Ostoich *et al.* (2013), with maximum panel displacement near the downstream boundary. Modes 2–4 are unstable and appear as high-order versions of fluttering panels with additional zero crossings of the downstream-localized panel displacement. Mode 5, in contrast, is stable and is characterized by panel deflections that are centered between the up- and downstream boundary conditions.

6. Conclusions

Convective and global stability analyses of a nominally flat panel show the appearance of instability modes affected by fluid-structural coupling. For a Mach 5.8 boundary layer grazing Hastelloy-X, a nickel-based alloy used in 1960s-era high-speed vehicles, the effects of structural compliance were observed in the convective stability analysis when the panel

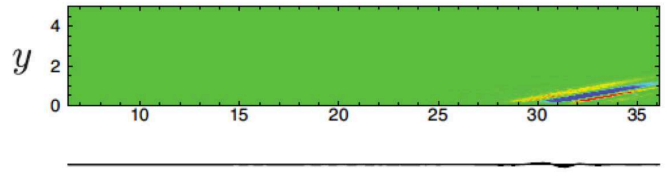

(a) Mode 1.

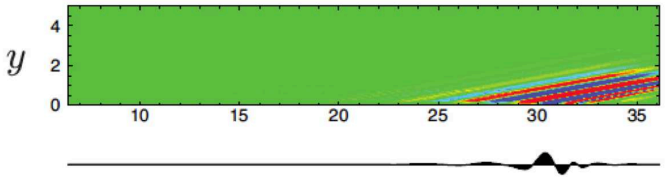

(b) Mode 2.

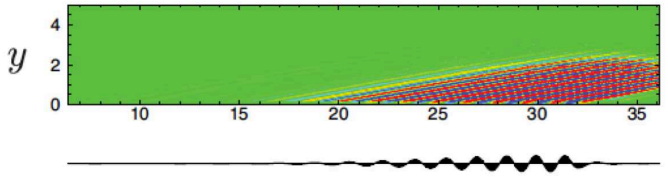

(c) Mode 3.

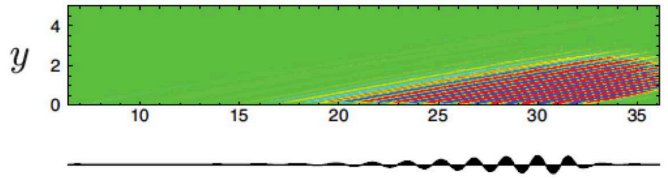

(d) Mode 4.

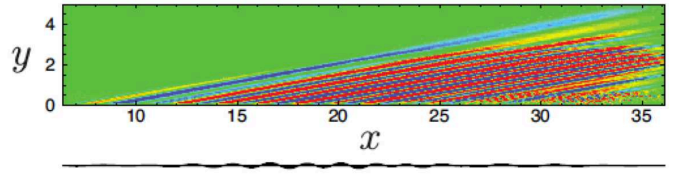

(e) Mode 5.

FIGURE 6. Five sample modes from the spectrum of Figure 5. Modes 1–4 are unstable while mode 5 is stable. The real part of the $\hat{v}$-velocity is shown in the fluid above the real part of the panel deflection $\hat{\eta}$.

thickness h^* satisfied the inequality $h^*\mathrm{R}/\ell^* < 10^{-1}$, where $\mathrm{R} = \sqrt{\mathrm{Re}_x}$ is the square root of the local Reynolds number and ℓ^* is the local Blasius lengthscale. The coupling increased the growth rate of the second Mack mode while stabilizing the first Mack

mode. When applying global stability arguments to a panel with up- and downstream boundary conditions a multi-branched spectrum was observed with several stable and unstable modes, the latter appearing to be similar to traditional panel flutter modes.

7. Acknowledgments

Contributions by Fabian Dettenrieder and Mahesh Natarajan, both from the University of Illinois at Urbana-Champaign, are gratefully acknowledged. Additional support from the Air Force Office of Scientific Research (Dr. Ivett Leyva, Program Officer) is also gratefully acknowledged.

REFERENCES

Bodony, D. J. & Natarajan, M. 2012 Controller selection and placement in compressible turbulent flows. *Proceedings of the Summer Program*, Center for Turbulence Research, Stanford University, pp. 35–42.

Carpenter, P. W. & Garrad, A. D. 1985 The hydrodynamic stability of flow over Kramer-type compliant surfaces. Part 1. Tollmien-Schlichting instabilities. *J. Fluid Mech.* **155**, 465–510.

Carpenter, P. W. & Garrad, A. D. 1986 The hydrodynamic stability of flow over Kramer-type compliant surfaces. Part 2. Flow-induced surface instabilities. *J. Fluid Mech.* **170**, 199–232.

Carpenter, P. W., Lucey, A. D. & Davies, C. 2001 Progress on the use of compliant walls for laminar-flow control. *J. Aircraft* **38**, 504–512.

Cebeci, T. & Smith, A. M. O. 1974 *Analysis of Turbulent Boundary Layers*, *Applied Mathematics and Mechanics*, vol. 15. Academic Press, New York, NY.

Culler, A. J. & McNamara, J. J. 2010 Studies on fluid–thermal–structural coupling for aerothermoelasticity in hypersonic flow. *AIAA J.* **48**, 1721–1738.

Dowell, E. H. 1970 Panel flutter: a review of the aeroelastic stability of plates and shells. *AIAA J.* **8**, 385–399.

Friedmann, P. P., McNamara, J. J., Thuruthiamatta, B. J. & Nydick, I. 2004 Aeroelastic analysis of hypersonic vehicles. *J. Fluids Structures* **19**, 681–712.

Kramer, M. O. 1957 Boundary-layer stabilization by distributed damping. *J. Aero. Sci.* **24**, 459.

Kramer, M. O. 1960*a* Boundary-layer stabilization by distributed damping. *J. Aero. Space Sci.* **27**, 69–69.

Kramer, M. O. 1960*b* Boundary-layer stabilization by distributed damping. *J. Am. Soc. Naval Eng.* **74**, 341–348.

Lucey, A. D. & Carpenter, P. W. 1995 Boundary layer instability over compliant walls: comparison between theory and experiment. *Phys. Fluids* **7**, 2355–2363.

Mack, L. M. 1965 Computation of the stability of the laminar compressible boundary layer. In *Methods in Computational Physics* (ed. B. Alder, S. Fernbach & M. Rotenberg), , vol. 4, pp. 247–299. Academic Press, New York, NY.

Mack, L. M. 1984 Boundary-layer linear stability theory. In *Special course on stability and transition of laminar flow*. AGARD Report AGARD-R-709.

Mattsson, K. & Werpers, J. 2016 High-fidelity numerical simulation of solitons in the nerve axon. *J. Comput. Phys.* **305**, 793–816.

Ostoich, C., Bodony, D. J. & Geubelle, P. H. 2013 Interaction of a Mach 2.25 turbulent boundary layer with a fluttering panel using direct numerical simulation. *Phys. Fluids* **25**, 110806.

Riley, Z. & McNamara, J. 2016 Interaction between aerothermally compliant structures and boundary layer transition in hypersonic flow. AIAA Paper 2016–1087, Presented at the 5th Dynamics Specialists Conference, San Diego, CA.

Riley, Z., McNamara, J. & Johnson, H. 2014 Assessing hypersonic boundary layer stability in the presence of structural deformation. *AIAA J.* **52**, 2547–2558.

Thuruthiamatta, B. J., Friedmann, P. P., McNamara, J. J. & Powell, K. G. 2002 Aeroelasticity of a generic hypersonic vehicle. *AIAA Paper* 2002-1209.

Wiplier, O. & Ehrenstein, U. 2001 On the absolute instability in a boundary-layer flow with compliant coatings. *Eur. J. Mech. B/Fluids* **20**, 127–144.

Zuchowski, B. 2012 *Predictive capability for hypersonic structural response and life prediction: Phase II – detailed design of cruise vehicle hot structure.* Air Force Research Laboratory. Tech. Rep. AFRL-RQ-WP-TR-2012-0280.